Applied Catalysis B: Environmental 237 (2018) 986–995

Contents lists available at ScienceDirect

Applied Catalysis B: Environmental

journal homepage: www.elsevier.com/locate/apcatb

CO/H_2 adsorption on a Ru/Al_2O_3 model catalyst for Fischer Trospch: Effect of water concentration on the surface species

E. Jiménez-Barrera[a], P. Bazin[b], C. Lopez-Cartes[c], F. Romero-Sarria[a,c,*], M. Daturi[b], J.A. Odriozola[a,c]

[a] Instituto de Ciencia de Materiales de Sevilla, Centro Mixto Universidad de Sevilla-CSIC, Avda. Américo Vespucio, 49, 41092 Sevilla, Spain
[b] Laboratoire Catalyse et Spectrochimie, Normandie Univ, ENSICAEN, UNICAEN, CNRS, Bd. Maréchal Juin, 14000 Caen, France
[c] Dpto. Química Inorgánica, Universidad de Sevilla, C/Prof. García González 1, 41012 Sevilla, Spain

ARTICLE INFO

Keywords:
Surface species
Infrared spectroscopy
Fischer Tropsch
Ruthenium
Water effect

ABSTRACT

Water presence and concentration strongly influence CO conversion and C_{5+} selectivity in the Fischer Tropsch reaction. In this work, the influence of the water concentration was investigated using a model Ru/Al_2O_3 (5 wt. %) catalyst. The surface species formed after CO and H_2 adsorption in dry and wet (different water concentrations) conditions were analyzed by FTIR. Firstly, water adsorption was carried out up to complete filling of the pores and then CO was put in contact with the catalyst. The absence of adsorbed CO species in these conditions evidences that CO diffusion in water controls the access of the gas to the active sites and explains the negative effect of high water concentrations reported by some authors. Moreover, the adsorption of a mixture of $CO + H_2 + H_2O$, being the water concentration close to that needed to have a monolayer, and a dry mixture of $CO + H_2$ were carried out and compared. Results evidence that water in this low concentration, is able to gasify the surface carbon species formed by CO dissociation on the metallic sites. This cleaning effect is related to the positive effect of water on CO conversion detected by some authors.

1. Introduction

The dependence of our current energy system on fossil fuels and their harmful effects on the environment have strengthen the development of renewable energy sources. This is the case of the second generation biofuels. The production of fuels from lignocellulosic biomass and wastes often involves catalytic processes, among these Fisher-Tropsch synthesis (FTS) is particularly important [1]. Carbon life-cycle assessment of these second-generation fuels entails important reduction of CO_2 emissions without extensive modification of the currently used engines, or fuel formulation and distribution, which is especially important in the automotive field. In this scenario, exploitation of different types of biomass takes special importance [2]. In a first step, biomass is gasified to syngas that further feeds a Fischer-Tropsch reactor, where a mixture of liquid hydrocarbons (C_{5+}) that may potentially be used in the same way as oil derivatives, is obtained [3].

Although the FTS is known since 1920 and industrial plants are currently under operation, improvements of the reactors and catalysts are still needed. Microchannel reactors, that may overcome diffusion limitations and heat transport effects on the selectivity are particularly interesting [4–6]. Moreover, the knowledge of the reaction mechanism may help to improve the global process and to design more performant catalytic solids. It is well accepted that the mechanism of FTS proceeds according to three main steps: (i) the initiation in which the CO molecule is dissociated and CH_x fragments are formed by hydrogenation, (ii) the propagation step with the formation of CH_x-CH_x species and (iii) chain termination and hydrocarbons desorption as a final step [7–9]. However, some aspects of the mechanism of this reaction are still under investigation [8,10,11].

The "carbide mechanism" was early proposed by Fischer and Tropsch. In this mechanism, CO is directly dissociated on the metal surface resulting in C* and O* adsorbed species, that are successively hydrogenated and initiate the chain growth [12]. However, according to recent studies, CO dissociation assisted by hydrogen must also be considered as an intermediate step for this reaction. A lower energy barrier for the CO dissociation in the presence of hydrogen was found on clean and H-precovered Fe (111) surface by Hou et al. [13]. These authors propose an adsorbed CHO intermediate for the H-assisted CO dissociation. Eq. (1) summarizes the proposed reaction path (X* = adsorbed species):

$$CO^* + 2H^* \rightarrow CHO^* + H^* \rightarrow CH^* + O^* + H^* \quad (1)$$

* Corresponding author at: Instituto de Ciencia de Materiales de Sevilla, Centro Mixto Universidad de Sevilla-CSIC, Avda. Américo Vespucio, 49. 41092 Sevilla, Spain.
E-mail address: francisca@us.es (F. Romero-Sarria).

https://doi.org/10.1016/j.apcatb.2018.06.053
Received 4 April 2018; Received in revised form 11 June 2018; Accepted 19 June 2018
Available online 23 June 2018

Both pathways (direct CO dissociation and H-assisted activation) have been evidenced for CO activation on cobalt catalysts [10], although the H-assisted activation of CO was proposed as the most favorable path [14]. Loveless et al. [15] studied the Ru-catalyzed FTS trying to unravel the mechanism for CO activation, either the direct C–O bond activation on vicinal vacant sites or the H-assisted activation of CO via its reaction with coadsorbed "H" atoms. Their results allow them conclude that CO is activated on Ru(111) terraces via the H-assisted path. The CO activation on Ru terraces suggests a strong dependence of the catalytic activity on the metallic particle morphology, as previously reported in the literature [16].

CO conversion in FTS strongly decreases with particle size (lower activity for smaller metallic particles) when metallic clusters are smaller than 10 nm [17,18]. For larger particles (> 10 nm), the CO conversion is not affected by the particle size. In the case of Co-based catalysts, the lower activity of smaller particles has been attributed to the formation of partially oxidized species. However, when Ru is used as active phase, the behavior of particles smaller than 10 nm is explained in terms of CO adsorption. The low coordination atoms, prevalent in small particles, are less active or that for these atoms the CO adsorption energy is too high. Moreover, large metallic particles improve the selectivity since step sites (numerous in small particles) inhibit chain growth [19]. Water, an unavoidable byproduct in the FTS, has a significant effect on the catalyst activity and selectivity. This effect, however, depends on the metal and support nature, the catalyst composition, and/or the preparation method used [20]. The effect of water on the CO conversion is not very clear from literature, but authors always agree on the improvement in C_{5+} selectivity by the presence of water either formed during reaction or added to the reactive mixture [21,22]. Most studies show that CO conversion increases in the presence of water on Co- [23,24] or Ru-catalyzed [25] FTS. However, catalyst oxidation in the presence of water has been proposed as responsible for a reduction of CO conversion on Fe [25] or Co catalysts [27,28]. In this latter case, the effect is particularly important for metal particle sizes below 4 nm [29]. Water may also affect the support: Storsæter et al. [30] report the effect of the presence of water on the support, which is especially important in the case of alumina, where water irreversibly deactivates the solid. Moreover, it has been reported that the formation of mixed oxide phases induced by the presence of water in the reaction stream affects the reducibility of the active phase and induces changes on the activity and selectivity of the metal catalysts [31–34]. Claeys et al. [35] tested a Ru/SiO_2 catalyst and found a positive effect of water addition. These authors affirm that water participates in the reaction mechanism, increases the catalyst activity and modifies the product distribution. The formation of methane is suppressed and chain growth favored, probably because water is an additional hydrogen source to the formation of monomers that participate in the chain growth. Other authors explain the water effects in terms of diffusivity of the products into the pores of the solid and to conclude that catalytic activity and products distribution depends on the pore size [36]. For Co-based catalysts, some works found a strong dependence between the water concentration and the pore size [25,37] and attributed this effect to diffusive aspects, because no modification of the surface species was detected after water addition [25]. However, in the presence of water Co-based catalysts deactivate. It has been observed for Co/SiO_2 catalysts that water addition to the inlet flow increases the selectivity to C_{5+}, but simultaneously deactivates the process by forming cobalt oxide species [37]. Bertole et al. [38] propose monomeric carbon as the active form responsible for the increase in the selectivity to C_{5+}, this through an increase of the active carbon concentration as a result of the decrease in the activation barrier for CO dissociation in the presence of water [21]. Ruthenium, however, is highly resistant to oxidation and therefore is very well suited for studying the effect of water on the FTS [20].

In this work, the effect of water has been investigated using a Ru/Al_2O_3 (5 wt.% Ru) working at 150 °C, the lowest temperature at which Ru is active in FTS. A Ru-based catalyst has been selected to carry out this study due to the high activity of this metal even at low temperature and pressure and that our experimental device doesn't permit to work at high pressure or very high temperatures. Moreover, the proved resistance of these solids to the oxidation by water is an interesting aspect to consider if water effect on the FTS is being investigated [39]. Initially, an isotherm of water adsorption was carried out in order to assure the complete filling of the pores. The CO adsorption was carried out both on the water saturated surface and on the dry surface in order to detect the effect of water at high concentration. Moreover, to observe possible differences in the surface species formed during the process, hydrogenation of CO saturated surface was compared with the surface species formed after adsorption of $CO + H_2$ and $CO + H_2 + H_2O$ mixtures. In this latter case, the water concentration was close to that needed to form a monolayer on the catalyst surface.

2. Experimental

The catalyst was prepared by wet impregnation. Commercial γ-Al_2O_3 (Sasol) was impregnated with 5 wt.% Ru, using $Ru(NO)(NO_3)_3$ solution (Johnson Matthey, CAS Number 34513-98-9) as precursor. The excess of solvent was eliminated at 100 °C and reduced pressure to dryness. The resulting solid was further air-calcined for 3 h at 400 °C. The calcination temperature was reached by linear heating at 10 °C min^{-1}. The prepared solid was characterized by different techniques. The calcination conditions were selected after a study of different calcination times and temperatures, regarding the textural properties and the stability of the resulting solids.

X-ray diffraction analysis (XRD) was performed on an X'Pert Pro PANalytical diffractometer using Cu Kα radiation (40 mA, 45 kV) over a 2θ range of 10-80° and a position-sensitive detector using a step size of 0.05° and a step time of 1 s.

Transmission electron microscopy (TEM) observations were carried out in a Philips CM200 microscope operating at 200 kV. The samples were dispersed in ethanol by sonication and dropped on a copper grid coated with a holey carbon film.

The nitrogen adsorption/desorption isotherm was measured by nitrogen adsorption at liquid nitrogen temperature (77 K) using a Micromeritics ASAP 2010 apparatus. The textural properties of the sample were studied using the Brunauer-Emmett-Teller (BET) and the Barret-Joyner-Halenda approaches. The experiments were carried out after degassing the sample for 2 h at 150 °C in vacuum.

Temperature Programmed Reduction (TPR) of the catalyst was performed under a 5% v/v H_2/Ar reactive gas stream at 50 mL min^{-1}. About 50 mg of sample was heated under this flow from room temperature (~20 °C) to 900 °C at 10 °C min^{-1}. A conventional quartz reactor coupled to a thermal conductivity detector (TCD) was used. The produced water was retained with a 13X molecular sieve. For quantitative analysis, the experimental H_2 consumption was determined upon calibration with CuO (Strem Chemicals, 99.999%).

CO adsorption on the Ru/Al_2O_3 catalyst was investigated using self-supported pellets (ca. 10 mg cm^{-2}; diameter of 13 mm), by Fourier Transform infrared (FTIR) spectroscopy. FTIR spectra were recorded in transmission mode with a Thermo Nicolet NEXUS 670 spectrophotometer, equipped with a MCT detector and accumulating 64 scans at a spectral optical resolution of 4 cm^{-1}. The experiments were performed by the means of a home-made IR cell recently developed in the LCS laboratory. This quartz IR cell is connected to a conventional vacuum-adsorption apparatus in order to 1) treat the sample with a residual pressure lower than 10^{-2} Pa) to control the addition of gas (H_2O, CO, H_2, …). More in details, the shape of the main part of the cell is a cylinder made of quartz that carries a 2-positions sample holder in its centre. One position allows the analysis of the self-supported wafer, while the second position is dedicated to collecting the IR spectrum of the gaseous phase. The heating system surrounding the quartz tube allows a maximum temperature of 773 K for the sample, whereas an air

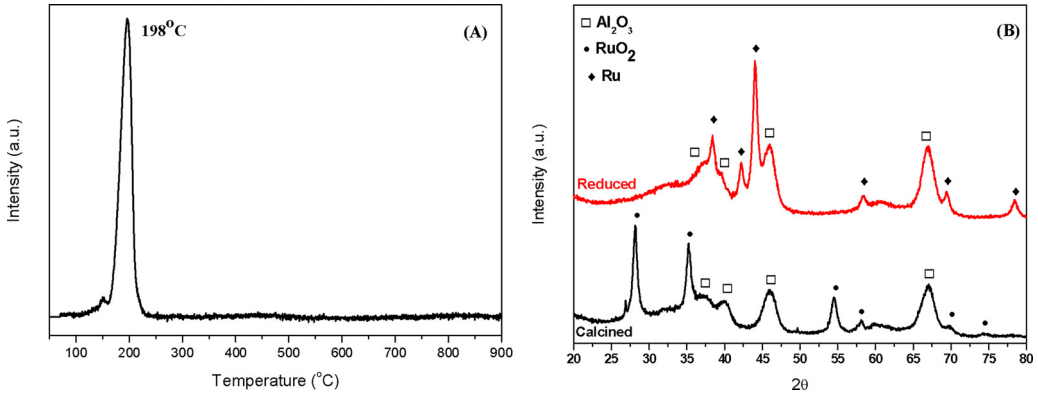

Fig. 1. TPR profile (A) and XRD of the calcined and reduced sample (B).

cooling system protects the two terminal KBr windows from heat damages. The cell is fixed on a motorized translation unit controlled by a software pilot that allows a programmed motion of the cell and the automatic acquisition of IR spectra, alternatively of the sample wafer and of the gas phase.

Previous to the CO adsorption at 150 °C, the sample was reduced under H_2 atmosphere by heating at 400 °C for 1 h.

3. Results and Discussion

The prepared catalyst was characterized by N_2 adsorption, XRD and TPR. The measured specific surface area of the catalyst is 173 m^2/g, the pore volume 0.4 cm^3/g and the average pore size 7 nm.

As evidenced by the TPR profile of the prepared catalyst (Fig. 1), 94.5% of ruthenium is reduced below 200 °C. Fig. 1 also presents the XRD patterns of the calcined and reduced catalyst. Together with the diffraction peaks of the alumina support (JCPDS 002-1420), diffraction lines corresponding to RuO_2 are evident (JPS 00-021-1172) in the calcined sample, whereas diffraction lines matching the structure of metallic ruthenium (00-006-0663) are observed upon hydrogen treatment at 400 °C for 3 h. Therefore, after the reducing treatment used to activate the catalyst, just Ru° is present in the sample. Scherrer analysis of the (110) diffraction line of the metallic phase let us calculate an average ruthenium particle size of 12.4 nm; this value is quite close to that measured by TEM on the activated sample (10.6 nm), Fig. 2.

The dispersion value may be estimated from this TEM measurement according to the following relationship [40]:

$$D = \frac{6.M}{\sigma.\ \rho.\ N_A.\ d_m} \quad (2)$$

where M is the atomic weight of ruthenium, ρ the density, σ the atomic surface area of the metal, NA the Avogadro's number, and d_m, the Ru particle size. According to this equation, Ru dispersion is 13%.

Water influences the catalytic activity of FT catalysts as evidenced by many authors. Two main aspects should be considered for understanding the role of water molecules on the activity and selectivity: the limitations on the diffusivity of syngas due to water pore filling [25,37] and the participation of water molecules in the reaction mechanism, either by the generation of alternative reaction pathways [37] or by cleaning active sites blocked by stable intermediates [25]. For these authors [25], water may modify the relative proportion of active and inactive forms of carbon on cobalt surfaces, although for them the mechanism remains unclear. Let's now verify which one of these hypotheses can be considered as the best explanation for the role of water.

3.1. H_2O + CO adsorption

As mentioned before, high water concentration may result in pore filling and therefore affects CO diffusivity altering this way the activity and product distribution. In order to test this effect an almost total saturation of catalyst by water was carried out upon activation. After catalyst activation in the IR cell, the Ru/Al_2O_3 sample was cooled down to RT and then submitted to successive doses of water. The IR spectra of the adsorbed phase as a function of the water coverage were recorded at RT (20 °C). Fig. 3 plots the amount of adsorbed water, measured as the height of the δ(H_2O) mode band at 1640 cm^{-1}, as a function of the water relative pressure up to P/P° ~0.8.

For studying the effect of the water surface layer on CO adsorption, 0.9 μmol of this gas was measured in a calibrated volume cylinder that connects to the IR cell. The water relative pressure into the cell just before CO addition was 0.7. The cell containing the CO (and water) was maintained at room temperature for one hour and then a heating program (up to 250 °C / 7.5 °C min^{-1}) was started. Once the temperature

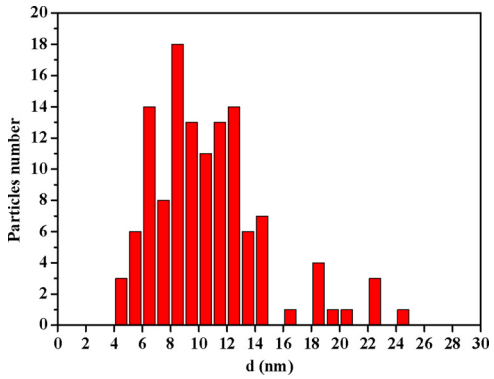

Fig. 2. Particle size distribution calculated by TEM analyses for the activated catalyst.

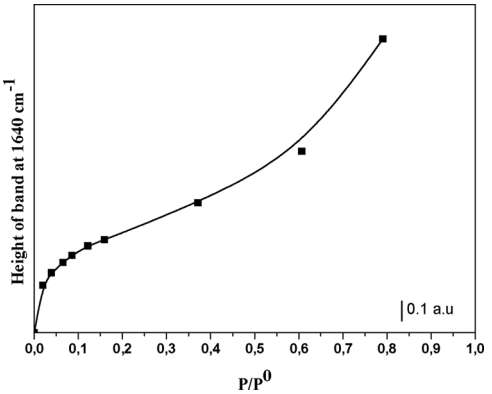

Fig. 3. Optical adsorption isotherm of water on Ru/Al_2O_3 at RT using the height of the δ(H_2O) characteristic vibration band of water.

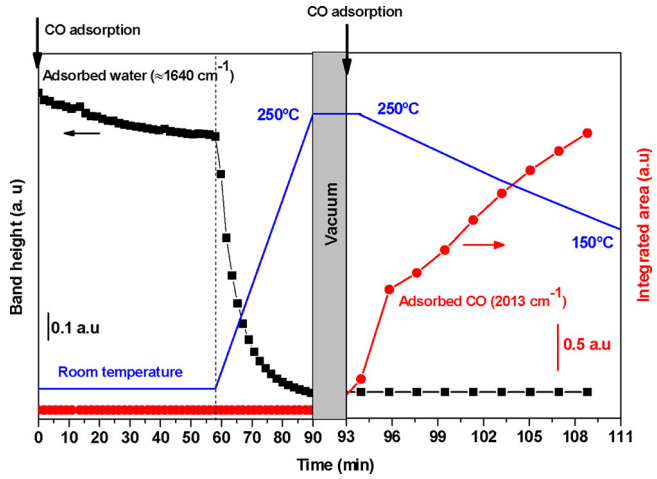

Fig. 4. Evolution of the intensity of the bands ascribed to adsorbed H_2O and CO as a function of time and temperature.

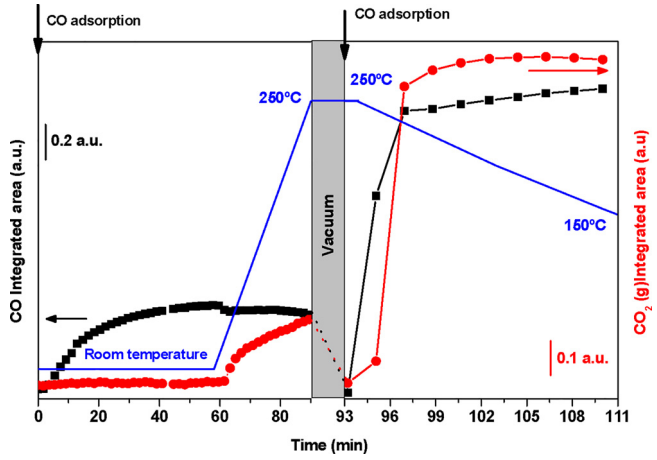

Fig. 5. Evolution of the intensity of the bands ascribed to gas phase CO and CO_2 as a function of time and temperature.

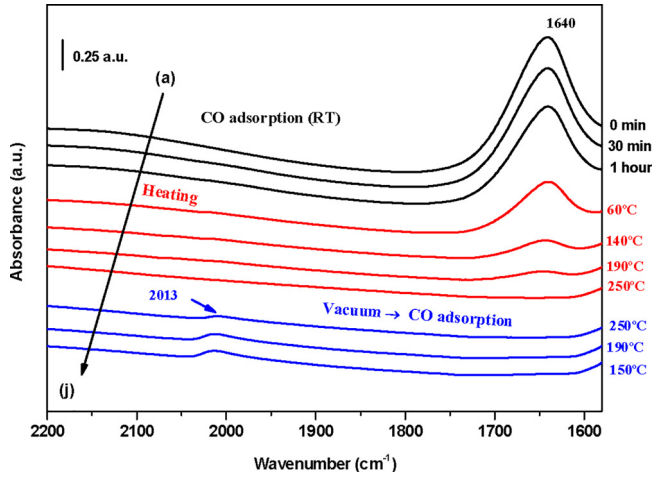

Fig. 6. Infrared spectra of adsorbed species upon CO interaction with water pore filled alumina surface as a function of time and temperature.

reached 250 °C, the sample was treated under vacuum and a new dose of CO was admitted into the cell. In these conditions, the temperature was progressively decreased. Evolution of adsorbed species and gaseous compounds in the cell as a function of the time and the temperature are shown in Figs. 4 and 5 respectively. Selected spectra of the solid at different moments of the experiment are shown in Fig. 6.

Upon CO introduction at RT (time 0 in Figs. 4–6), the partial pressures of H_2O and CO were 0.91 and 0.09 tor, respectively; thus, the equilibrium water pressure is $P/P^\circ \sim 0.6$. During the 60 min at room temperature, the amount of adsorbed water, measured through the intensity of the $\delta(H_2O)$ mode band at 1640 cm^{-1}, smoothly decreases to a level that corresponds with the amount adsorbed at $P/P^\circ \sim 0.6$ (Fig. 4 left panel), while at the same time, the amount of CO in the gas phase slowly increases with time (Fig. 5 left panel). This indicates that the rate of mixing of CO and water, even in the gas phase, is slow. Bands that could be ascribed to adsorbed CO species are completely absent (Fig. 6, spectra a–c), but the CO dissociation on the metal to produce species not visible to IR (as C* species) cannot be discarded.

At RT, as it can be observed in Fig. 3, the intensity of the $\delta(H_2O)$ band upon water interaction clearly indicates water pore filling ($P/P^\circ = 0.75$). In these conditions, CO adsorption is hindered (Fig. 4), supporting the negative effect of water on CO diffusivity at RT, which is evidenced by the absence of CO absorption bands in the IR spectrum after 60 min at this temperature (Fig. 6). At this point, a temperature program was imposed to the cell, since high temperatures are required to remove the molecularly adsorbed water from the surface. The temperature in the closed reaction volume was increased at 7.5 °C·min^{-1} up to 250 °C, which results in an increase of the pressure by *ca.* 20% accounting for the thermal desorption of the water molecules and the apparent volume modification, since the average temperature of the reaction vessel has slightly increased. Upon heating, the amount of molecularly adsorbed water, measured through the intensity of the $\delta(H_2O)$ mode at around 1640 cm^{-1}, continuously decreases but adsorbed CO species remain undetected. On increasing the reaction temperature, CO diffusion starts to be favored, as observed by the evolution of CO_2 in the gas phase at relatively low temperatures, even in the absence of adsorbed CO species (Figs. 4 and 5). Finally, the IR cell was outgassed at 250 °C and CO was admitted at this temperature (0.9 µmol, as previously). As can be seen in Fig. 5 there is an immediate production of CO_2 in the gas phase. The CO/CO_2 gas phase molar ratio reaches a constant value at temperatures close to 200 °C ($CO/CO_2 = 0.13$) and hardly changes on decreasing temperature. For calculating this ratio the molar extinction coefficients for CO and CO_2 from [41] were used. Only after introduction of the second dose of CO into the cell and when the sample temperature reaches ~190 °C (Fig. 6 spectra h–j), CO adsorbed species are clearly observed. At this temperature the $\delta(H_2O)$ mode is absent and a band peaking at 2013 cm^{-1} appears. According to Hadjiivanov et al. [42], this band may be assigned to CO adsorbed close to carbon covered Ru sites. Dulaurent et al. [43] observed a red-shift of the linear CO adsorbed band at 2047 cm^{-1} down to 2008 cm^{-1} upon heating a CO-covered Ru/Al_2O_3 surface; they ascribed this shift to carbon deposition as a result of CO dissociation.

This experience demonstrates that filling the support pores with water reduces CO diffusivity, therefore hindering its access to the active sites, at least at the pressures used in this work. This observation may explain the strong influence of the pore size on the CO conversion and product distribution observed in slurry reactors by some authors [44] that ascribed this influence to the diffusion of CO and H_2 in the slurry solvent. Delgado et al. [45] drew similar conclusions on studying the effect of the solvent nature in the FTS activity in slurry reactors. They conclude that the low solubility of syngas in water causes low CO conversions and the formation of short chain products. However, despite the fact of the absence of absorption bands for adsorbed CO, the formation of gas phase CO_2 is observed upon heating at temperatures well below 190 °C (Fig. 5). Several explanations may account for this fact: i) the water-gas-shift reaction; ii) the Bouduard reaction [46,47] and iii) the reaction of CO with the oxidized surface of ruthenium upon water interaction [52]. Taking into account that CO_2 appears at temperatures close to RT and that the formation of surface intermediates on the Ru surface requires the presence of adsorbed CO (not observed), the most likely explanation is the last one. Water may dissociate on the

$$Ru^0 + H_2O \longrightarrow Ru - O + H_2 \text{ Equation (2)}$$

$$Ru - O + CO \longrightarrow Ru^0 + CO_2 \text{ Equation (3)}$$

Scheme 1. Model for the CO_2 production by CO reaction with the surface water layer.

ruthenium surface at temperatures as low as −100 °C as stated by Michaelidis et al. [48]. DFT studies of the adsorption of H_2O monomers and water bilayers on Ru{0001} allow these authors, in agreement with Fiebelman [49], to state that a partially dissociated OH-H_2O is thermodynamically more stable than any water bilayer on Ru{0001}. The energy barrier for water dissociation in a bilayer was calculated to be 0.5 eV, which is 0.3 eV below the energy required for dissociating a H_2O monomer on the ruthenium surface. Experimental evidences for water dissociation at low temperature on multilayer water adsorption were previously reported [50,51]. Therefore, upon water adsorption at P/P° > 0.7, formation of a water multilayer and hence the formation of a RuO_x surface layer may be expected, then CO molecules reaching the surface just reduce this surface layer resulting in the formation of gas phase CO_2. Scheme 1depicts a model for this process.

$$Ru^0 + H_2O \longrightarrow Ru{-}O + H_2 \quad (3)$$

$$Ru{-}O + CO \longrightarrow Ru^0 + CO_2 \quad (4)$$

The role of the carboxyl species as intermediate in the WGS reaction has been previously highlighted [51]. However, the Boudouard reaction cannot be disregarded.

$$2CO + * \rightleftharpoons CO_2 + C^* \quad (5)$$

Panagiotopoulou et al. [53] on running the CO methanation reaction observed a low temperature evolution (~100 °C) of CO_2 that cannot be ascribed to the WGS reaction. They proposed the reduction of partially oxidized Ru present on the catalyst surface, although there is no explanation of the origin of these oxidized species. Moreover, these authors indicate that the Bouduard reaction is also possible but they overruled this hypothesis at least as the main contribution for the CO_2 evolution at low temperatures. In our case, CO adsorption at 250 °C on a dehydroxylated surface demonstrates that the Bouduard reaction takes place at this temperature (Fig. 5). Fig. 4, shows that the CO coverage (band peaking at 2013 cm^{-1}) continuously increases on decreasing temperature. The position of this band indicates that CO adsorbs on Ru sites close to carbon deposits [42].

3.2. CO, H_2 and H_2O co-adsorption

In addition to the above-mentioned effects of water on the diffusivity of syngas, some authors [35] claim for the participation of water in the reaction mechanism of the FTS on Ru catalysts. On the other hand, in the case of Co-based catalysts, Krishnamoorthy et al. [25] could not found any difference on adsorbed surface species upon water addition to syngas. To shed some light on the possible participation of water species on the mechanism of the FTS reaction on our Ru/Al_2O_3 catalyst, we have studied the nature of the CO adsorbed species upon adsorption of a 1:1 CO:H_2 mixture to which water was added. Water partial pressure in this mixture was enough to form a monolayer on the catalyst surface (P/P° ~ 0.25 in Fig. 3). To identify the effect of water, the nature of the surface species formed upon CO adsorption as well as CO and H_2 co-adsorptions were also studied.

First, we studied by FTIR the adsorption of CO at 150 °C on the activated catalyst and the time evolution of the adsorbed surface species. Fig. 7 presents a selection of these surface species spectra. For clarity, difference spectra are shown. The reference spectrum for these differences was taken after activating the catalyst at 400 °C for 1 h and further cooling down the catalyst to 150 °C under vacuum.

The spectrum taken immediately after the admission of 60 torr of CO into the cell, kept at 150 °C, is shown in Fig. 7, bottom line black trace. Upon adsorption, a main band at 2047 cm^{-1} assigned to CO linearly adsorbed on metallic sites is observed [23,54]. The intensity of this band increases with time and shifts from 2047 to 2056 cm^{-1} on increasing the CO coverage, as previously reported [55]. Besides this, two new bands of very low intensity at 2157 and 2144 cm^{-1} and a low intensity shoulder at ~2090 cm^{-1} develop after 30 min under the CO atmosphere. These bands indicate the existence of oxidized Ru sites [23]. For Ru/Al_2O_3 catalysts, bands at 2140 and 2072 cm^{-1} have been reported for $Ru\delta^+$-$(CO)_3$ and at 2150 and 2088 cm^{-1} for Ru^+-$(CO)_2$ species [42]. According to the TPR profile (Fig. 1A) only metallic Ru should be expected on the catalyst surface after the high temperature reduction pretreatment. Therefore, the evolution of these bands indicates the oxidation (at least partially) of metallic sites under CO at 150 °C. Although this may be surprising since CO is a reducing agent, the high capacity of metallic Ru to dissociate CO into adsorbed C* and O* species should result in partially oxidized ruthenium by the presence of O–adsorbed species [56]. Loveless et al. [15] suggest that these bands account for the presence of < 6 nm Ru particles.

Moreover, bands at 3620, 1697, 1480, 1437 and 1228 cm^{-1} are also clearly observed. The intensity of these bands increases while the intensity of the hydroxyls band peaking at 3770 cm^{-1} decreases (Fig. 7B). The first set of bands is due to bicarbonate species adsorbed on alumina [57]. The presence of bands at 1480 and 1437 cm^{-1} evidences the coexistence of the named B1 and B2 bicarbonate species, respectively [58]. Bands at 1697 cm^{-1} and 1228 cm^{-1} appear at similar positions for both types of bicarbonates and only a shift of 8 and 5 cm^{-1} is produced when B1 bicarbonates are transformed into the B2 ones. According to Morterra et al. [58], B2 bicarbonates are mainly formed at the expense of hydroxyls with ν_{OH} = 3770 cm^{-1} with the participation of those at 3690 cm^{-1}, in good agreement with our observations. Since bicarbonates are formed by interaction of CO_2 with these hydroxyls groups and in our case only CO has been introduced into the cell, the possible presence of CO_2 has to be analyzed. The spectra of the gas phase as a function of time under CO atmosphere (not shown) evidence the presence of both CO and CO_2. A possible source for the latter is the Boudouard reaction (Equation (5), which implies the formation of carbon species on the surface. Some authors also propose the formation of CO_2 by direct reaction between CO and hydroxyls of the support according to the following process [59]:

$$CO + OH \longrightarrow CO_2 + \frac{1}{2}H_2 \quad (6)$$

This idea is in good agreement with the catalytic activity of Ru-based catalysts in the water gas shift reaction [60,61] and may also be considered.

A semi-quantitative analysis of the concentration of CO and CO_2 in the gas phase by integration of their corresponding IR bands is shown in Fig. 8 as a function of time. The CO_2 concentration slightly increases with time reaching a plateau at ~60 min, while the CO concentration is hardly modified; taking into consideration the differences in the IR sensitivity for CO and CO_2 it may be concluded that the reaction does not occur to a large extent at 150 °C. The CO-to-CO_2 area once CO_2 reaches the plateau, is 1.38 (the absolute areas for the CO and CO_2 signals are 1.8 and 1.3 a.u, respectively), which taking into consideration the molar extinction coefficients for CO and CO_2 [41] accounts for a P_{CO2}:P_{CO} ratio close to 0.1.

The nature of the adsorbed species also changes on increasing time: B2 bicarbonates disappear between 20 and 70 min, B1 bicarbonates increases up to 70 min and then decreases and bands typical of formates at 1593 (ν_{as}OCO), 1397 (δCH) and 1372 (ν_sOCO) cm^{-1} continuously grow. The presence of formate is also confirmed by a new band appearing at 2906 cm^{-1} assigned to the ν(CH) mode of these species. Evolution of B1 and B2 bicarbonates, formates and hydroxyls, represented by the height of the bands at 1437 cm^{-1}, 1480 cm^{-1}, 1593 $cm^{-1}$and 3520 cm^{-1} respectively, are show in Fig. 9A. In this

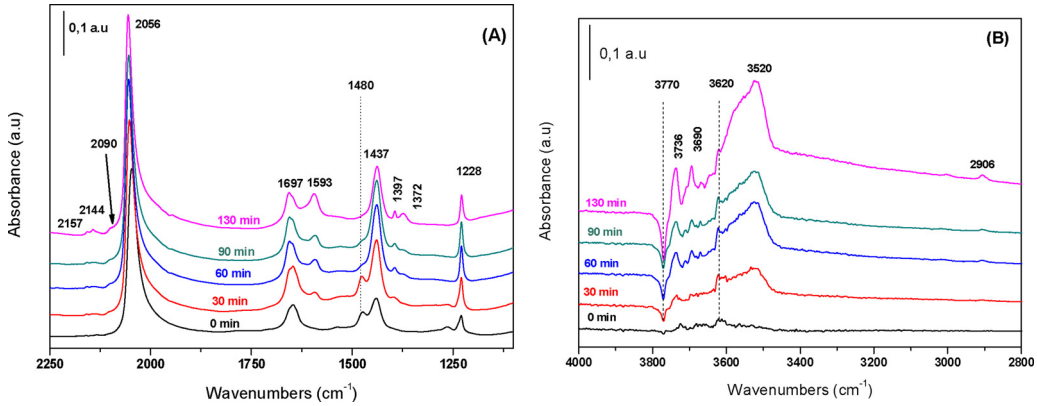

Fig. 7. Time evolution of adsorbed surface species under CO atmosphere at 150 °C in regions 2250–1200 cm^{-1} (A) and 4000–2800 cm^{-1} (B).

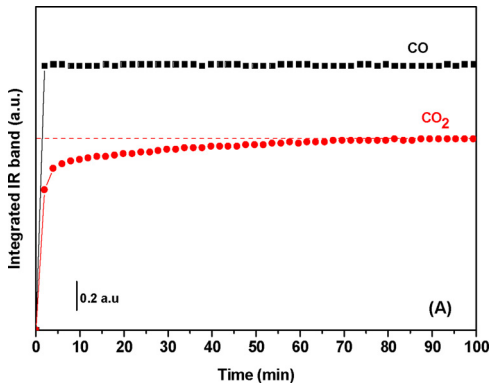

Fig. 8. Integrated areas of characteristic IR band of CO and CO_2 (gas) as a function of the time under CO atmosphere at 150 °C.

figure, the disappearance of B2 bicarbonates between 20–70 minutes is observed. Evolutions of bands typical of both species have been analyzed in this time interval and the spectra (recorded every 7 min) are shown in Fig. 9B. The presence of an isosbestic point (* in figure) evidences the transformation of B2 into B1 species, which is related to a modification of the surface (decreasing of defects number, according to Morterra et al [62].). In the hydroxyls region, it is observed (Fig. 7B) the decreasing of band at 3770 cm^{-1} (associated to the presence of crystallographic defects in the coordination sphere of aluminum) and the growth of those at 3736 and 3690 cm^{-1} attributed to $(Al_{VI})_2OH$ and $(Al_{VI})_3OH$, respectively [63]. This fact, together with the presence of an intense band at 3520 cm^{-1} due to adsorbed water, suggests that water is formed in these conditions.

Bicarbonate decreasing and water formation may by explained according to [59]:

$$HCO_3^- + H_2 \rightleftharpoons HCOO^- + H_2O \quad (7)$$

Hydrogen required by this reaction has to be produced by the formate species in the metal-support interphase decomposition as previously proposed [53]. Early studies on the interaction of CO with the surface of Rh/ZrO_2 catalysts have pointed out that CO adsorbed on Rh may react with surface hydroxyls groups of ZrO_2 resulting in the formation of adsorbed formate species [64]. On the other hand, the reaction of gas phase CO with OH radicals has been demonstrated as the principal source of CO_2 in hydrocarbon oxidation [65]. Carbon dioxide formation may occur through a HOCO (carboxyl) intermediate that further decomposes into CO_2 and H_2 [66]. This HOCO species is a key intermediate in the water gas shift reaction [67]. Politano and Chiarello [68] identified HOCO species upon coadsorption of water and CO on Pt_3Ni surfaces at 100 K. These species further decompose into CO_2 and H_2 at temperatures above 438 °C on the metallic surface allowing these authors to postulate carboxyl species as intermediates in the WGS reaction. Therefore, the reaction of CO adsorbed on the Ru surface with OH species at the metal support interface may result in H_2 production. Senanayake et al. [52] also support this hypothesis discarding the decomposition of formate species as hydrogen source upon interaction of CO with hydroxyl groups.

In Scheme 2, ways (A) and (B), the possible reaction steps after CO interaction with the catalyst surface (* = adsorbed species) are shown.

Therefore, we can consider the reduction of bicarbonates (B1) to formates and water through interaction of CO species with adsorbed hydroxyl groups, being the formed water the responsible for the growth of the bands at 3739, 3690 and 3520 cm^{-1}. This idea is in good agreement with the simultaneous increase of the intensity of the formate and hydroxyls bands while the B1 bicarbonate bands decrease,

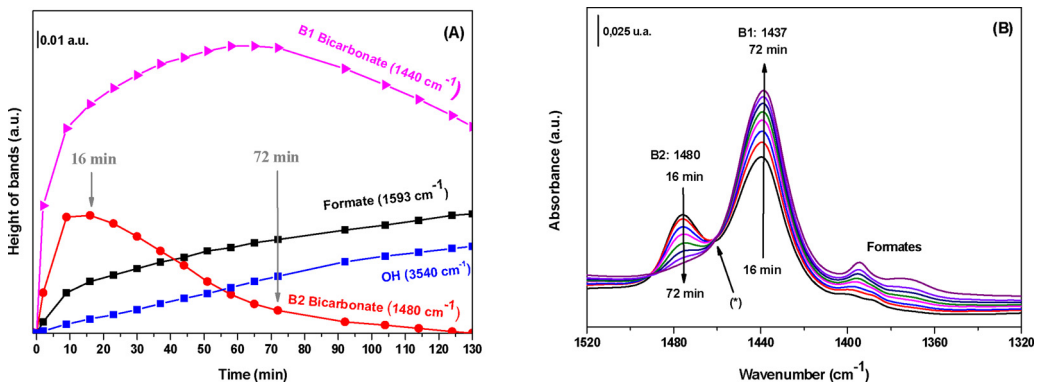

Fig. 9. (A) Evolution with time of B2 and B1 bicarbonates, formates and hydroxyls adsorbed on Ru/Al_2O_3 under CO atmosphere at 150 °C; (B) Evolution of bands typical for B1 and B2 bicarbonates between 16 and 72 min (every 7 min).

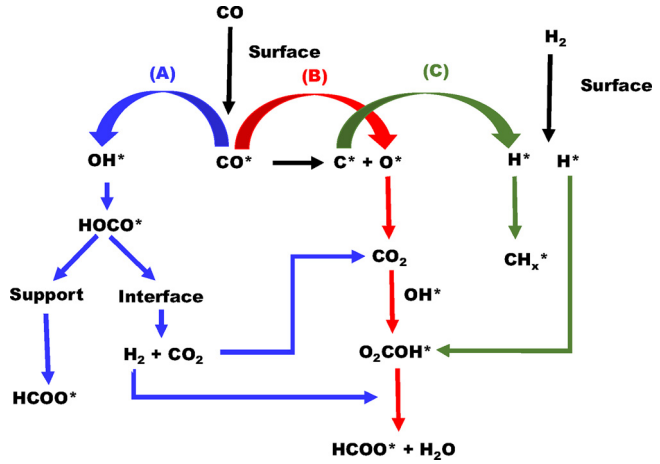

Scheme 2. Possible reaction steps after CO adsorption on the catalyst surface in absence (A and B) and presence (C) of hydrogen.

Fig. 9. In our case, bicarbonate species disappear with time, but its direct decomposition may be discarded since CO and CO_2 concentrations are constant (see Fig. 8). Therefore, bicarbonate reduction by the formed H_2 seems to be the most probable route to explain the disappearance of the band at 1437 cm^{-1} and the growth of hydroxyl bands.

Once the surface species under CO atmosphere were stabilized, hydrogen was introduced into the IR cell (H_2/CO = 1) at constant temperature (150 °C). Evolution of surface species with time is shown in Fig. 10.

It is clearly observed that after hydrogen admission in the cell, the band at 2056 cm^{-1} shifts to 2032 cm^{-1} and becomes broader. The shift to lower frequencies is due to hydrogen adsorption on the surface that increases the backdonation ability of the Ru sites [69]. On increasing this backdonation capacity, CO dissociation may become easier, resulting in CO species adsorbed close to carbon deposits, which will also result in a redshift from the original 2056 cm^{-1} band. The total area of linear CO band decreases after hydrogen adsorption suggesting a lower number of carbonyl species on the surface. Two facts have to be considered: the hydrogenation of the carbonyls or the CO desorption. The analysis of the gas phase spectra shows that the integrated areas of both CO and CO_2 increase of about 25% after hydrogen adsorption (CO/CO_2 area ratio is not modified) indicating that CO desorption is the most probable fact. Ciobica et al. [70] calculated the adsorption energies of CO on different sites of a Ru surface and studied the effect of the presence of H species on them. They found that the CO adsorption energies might become positive on some types of sites (meaning that the gas phase is the most favorable state) when the amount of "H" species exceeds that of CO, in good agreement with our observations. The increase of the CO_2 integrated area suggests not only the carbon monoxide desorption but the CO reaction, probably with adsorbed oxygen fragments previously produced by the CO dissociation, resulting in gas phase CO_2.

Simultaneously, in the region from 3100 to 2700 cm^{-1}, bands at 3002, 2964, 2926, 2908 and 2856 cm^{-1} due to ν(CH) vibrations appear. Note that the band at 2906 cm^{-1} (observed at time 0 min and growing with time) was already observed when the surface saturation in CO being assigned to the C–H stretching of formate species together with bands at 1593, 1397 and 1372 cm^{-1}. The band at 3002 cm^{-1} that appears at the same time must be ascribed to a combination of the asymmetric stretching of the O—C and the C–H bending [71]. It is worth noting that under hydrogen atmosphere, bands due to bicarbonate species (only B1 type remains on the surface) decrease, while those due to formate increase, suggesting the reduction of bicarbonate by hydrogen, as previously proposed. Moreover, under hydrogen atmosphere, an increase of the intensity of the band at 3520 cm^{-1} is also observed, similarly to that on Fig. 7, and confirming the water formation. Bands at 2926 and 2856 cm^{-1} may be attributed to the asymmetric and symmetric ν(C–H) vibrations of CH_2 saturated groups. The feature at 2964 cm^{-1} is assigned to CH_3 groups [72].

Given that CO dissociation on Ru has been confirmed during the first step of the experiment (surface saturation with carbon monoxide and CO_2 observation) and that the CO desorption explains the decrease of the carbonyl band intensity, it can be stated that the observed ν(C–H) vibrations correspond to species formed upon hydrogenation of adsorbed carbon species at 150 °C; that is, formed through the "carbide mechanism". Considering the conditions in our IR cell (low pressure and low H_2/CO ratio) and the strong metal-carbon bond, a high extent of chain growth reactions cannot be expected [73,74].

The coadsorption of a mixture of CO-H_2 (H_2/CO = 1) on Ru/Al_2O_3 at 150 °C results in an IR spectrum (Fig. 11) quite close to that obtained after admitting H_2 in a CO covered surface shown in the previous section.

Immediately after admitting the gas mixture into the cell (black spectrum), a band at 2054 cm^{-1} is detected. With time, this band shifts to lower frequencies (2035 cm^{-1}) and becomes broader, as previously observed. The detection of very low intensity bands at 2156, 2143 and 2097 cm^{-1} (CO adsorbed on $Ru\delta^+$ sites) [23] indicates that a certain CO fraction is being dissociated generating O* fragments able to oxidize the metal and partially covering the metallic surface with carbon. The shift in the CO adsorption band also suggests an increase in the backdonation process as previously stated, due to the chemisorption of hydrogen on the metal surface [70] and/or to the presence of carbon deposits that results in a decrease of the CO adsorption frequency to values as low as 2010 cm^{-1} [42].

In the region 1800-1200 cm^{-1}, the observed species are similar to those formed after CO saturation (bicarbonates and formates) but now, B2 bicarbonates (1480 cm^{-1}) are not detected. As it has been

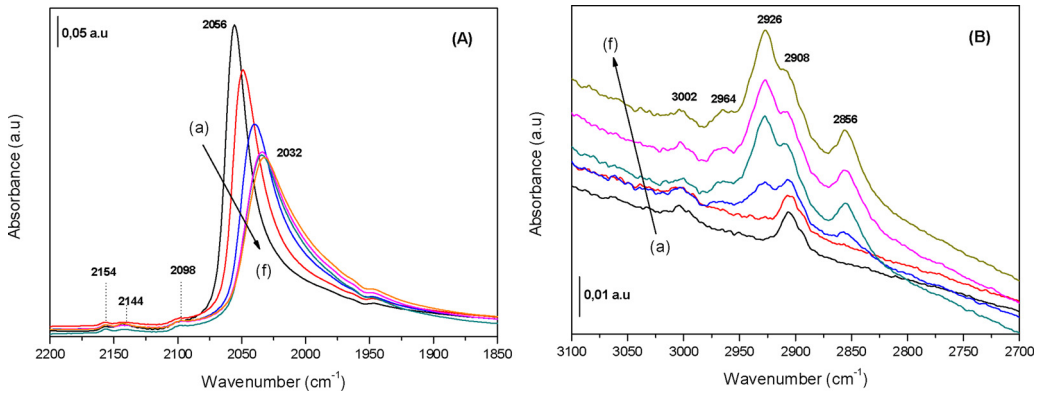

Fig. 10. Spectrum evolution of the CO saturated surface after H_2 adsorption at 150 °C (a) 0 min, (b) 7 min, (c) 20 min, (d) 30 min, (e) 40 min (f) 50 min.

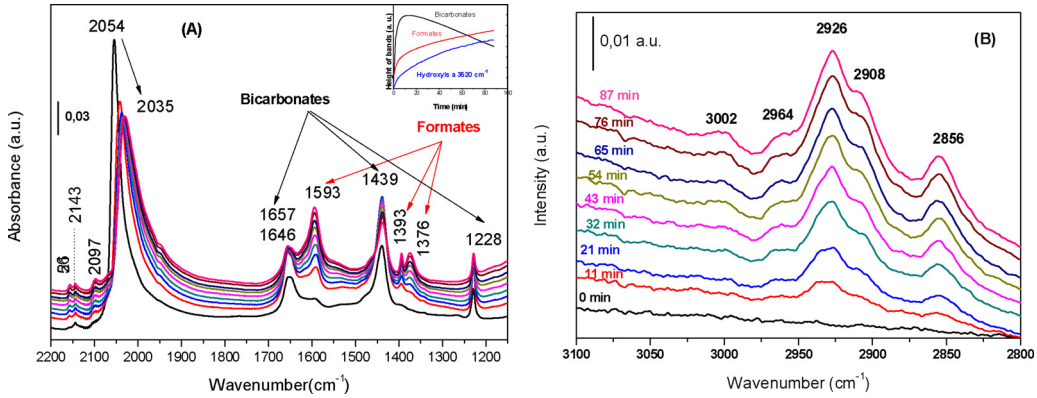

Fig. 11. Evolution of surface species after the coadsorption of CO-H_2 on Ru/Al_2O_3 at 150 °C (inset: evolution with time of the band intensities for bicarbonates, formates and hydroxyls).

previously said [58], this type of bicarbonate is formed on defective tetrahedral Al_{IV} sites of partially dehydroxylated alumina. The absence of the band at 1480 cm^{-1} suggests that hydrogen or other species occupy these defects inhibiting the formation of B2 species. As previously, bicarbonates are immediately formed and then, bands of formates develop. A deep analysis of the evolution of the bands indicates that the surface amount of bicarbonate and formate species increases during the first 10 min. A further increase in the reaction time results in a decrease of the intensity of the bicarbonate bands together with an increase of the intensity of the formate bands (inset in Fig. 11A). Moreover, an intense band at 3520 cm^{-1} develops in parallel to the formate band evolution; this confirms the reduction of bicarbonate species by hydrogen to give formates and water (Eq. (7)).

The evolution of gas phase CO and CO_2 is shown in Fig. 12. In this figure, the areas under CO and CO_2 bands are shown as a function of time.

A continuous decrease in the area of the gas phase CO bands is observed reaching a plateau at *ca.* 55 min. The area under the CO_2 band rapidly increases reaching a constant value after ~8 min reaction. This behavior is consistent with the Bouduard reaction that implies CO dissociation and further reaction of the adsorbed oxygen species with CO (Scheme 2, red way).

However, this process seems to end up after 8 min of reaction since the CO_2 concentration remains unaltered from this point. The continuous decrease of the CO concentration up to 45 min after the reaction begun implies that other processes are involved in CO consumption.

Taking into account the evolution of the surface species, it is clear that the equilibrium between species in the gas phase and those on the surface is slowly attained when hydrogen and CO are coadsorbed. This fact may be related with a lower number of available surface sites for CO interaction due to the presence of hydrogen. The repulsive interaction between adsorbed CO and H considered by some authors [70] provokes the modification of the adsorption energies on metallic surfaces and may explain the observed trend in the gas concentrations.

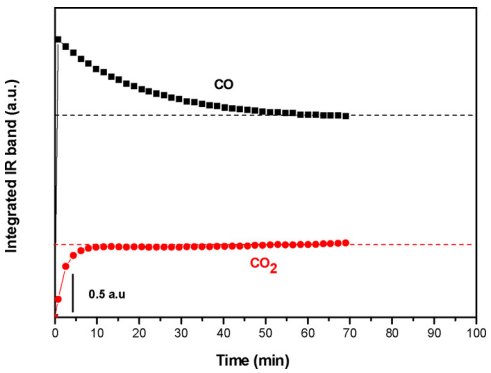

Fig. 12. Evolution of integrated IR bands of CO and CO_2 (gas) with the time under atmosphere of CO + H_2 at 150 °C.

Moreover, once stability is reached, the P_{CO2}:P_{CO} ratio is close to 0.045, indicating a lower production of CO_2 than previously, probably due to the occupancy of some surface sites by hydrogen. This fact also indicates a lower amount of adsorbed carbon species on the surface.

In the ν(C–H) region, bands similar to those obtained after hydrogenation of the surface saturated in CO are observed, indicating that similar species are formed.

The continuous increase in the intensity of the bands in the 3100 to 2700 cm^{-1} region confirms the continuous increase in the surface concentration of formate species (bands at 2906 and 3002 cm^{-1}) as well as an increase in the concentration of surface CH_x species (CH_2 and CH_3 bands at 2964, 2926 and 2856 cm^{-1}). This suggests that the decrease in the gas phase concentration is the result of CO dissociation on the metal surface that is further hydrogenated to CH_x species. Besides this, gas phase CO may react with the adsorbed O* species resulting in CO_2 that reacts with surface hydroxyls of the alumina, causing the increase in the concentration of surface bicarbonates and formates. Moreover, the metallic surface is progressively covered by CH_x species (see Scheme 2).

3.3. (CO-H_2-H_2O) adsorption

When water (P/P_0 = 0.25 in Fig. 2A: close to monolayer) is added to the mixture CO-H_2 and adsorbed on the activated sample, we observe a similar evolution of the carbonyls band (initially at 2055 cm^{-1}, with a shift to 2030 cm^{-1} with time), but bands above 2100 cm^{-1}, assigned to oxidized Ru are not detected. It is interesting to note that bicarbonate species are not at all detected in this case, meaning that the presence of water inhibits their formation or that this species undergo a rapid transformation in these conditions. However, a band at 1466 cm^{-1} due to carbonate species is now detected.

Szanyi et al. [75], studied the interaction of CO and CO_2 with alumina annealed at different temperatures. They observed that the CO adsorption at room temperature on alumina does not provoke the formation of carbonates or bicarbonates. However, the CO_2 adsorption on metal free alumina generates bicarbonates B1 and B2 and carbonate species. As previously explained, the presence of defects on the alumina support is needed for the bicarbonate formation [58] and its absence indicates that water is occupying these sites.

The evolution of CO and CO_2 in gas phase is shown in Fig. 13.

In this case, after 35 min the P_{CO2}:P_{CO} ratio is close to 0.045, roughly the same as in the case of coadsorption of CO + H_2, suggesting a similar number of surface sites available for the Boudouard reaction. However, as the time increases, the CO_2 amount in the gas phase

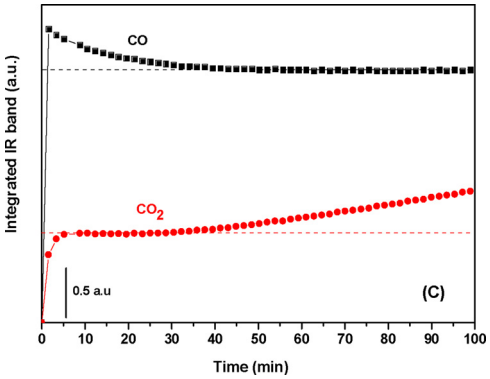

Fig. 13. Evolution of integrated areas of characteristic band of CO and CO_2 (gas phase) with the time when Ru/Al_2O_3 under an atmosphere of $CO + H_2 + H_2O$ at 150 °C.

continuously increases without modification of the CO concentration. Therefore, we can affirm that water is involved in the gasification of carbonaceous rests formed on the surface. Given that adsorbed carbon is invisible by infrared, the amount of CO_2 in the gas phase is the only proof of its gasification. However, previous experiences (not shown in this paper) evidence a loss of about 33% of adsorption sites after CO adsorption on a dry catalyst, while this loss was only of about 8% when CO was adsorbed on a wet solid. Although the water amount used in these experiments is very low, the results points to an improvement of the solids stability, at least regarding the coking.

3.4. Comparation of results

In all the experiments, a certain quantity of CO_2 has been produced and it has been related to the formation of adsorbed carbon by the Boudouard reaction. These species are hydrogenated producing the bands observed in the region of ν(C–H) vibration. Therefore, a higher amount of CO_2 produced must result in a higher amount of CH_x species. Moreover, the intensity of carbonyl bands is proportional to the number of metallic sites on the surface. Keeping these ideas in mind, we will analyze the obtained results. In Fig. 14, the integrated areas of carbonyls and the height of the band at 2926 cm^{-1} (ν_{asym}(C–H) vibration of CH_2) in each one of the experiments are presented as a function of time. From this figure, some interesting observations have to be remarked.

When the surface is firstly saturated with CO, a high amount of carbonyl is formed initially (all the metallic sites are able to adsorb CO) and decrease after H_2 admission, as previously discussed. In this case, the measured area of CO_2 (1.3 a.u.) indicates that the amount of adsorbed carbon on the surface is the highest, in good agreement with the highest intensity of the band at 2926 cm^{-1} (Fig. 14).

In the case of $CO + H_2$ co-adsorption on the activated sample, bands of carbonyls are of very low intensity and decrease with the time, suggesting a lower amount of CO adsorbed on metallic sites and a lower CO_2 production by the Boudouard reaction (0.9 a.u.). This explains the lower intensity of the ν(C–H) band.

Finally, if water is added to the mixture $CO + H_2 + H_2O$, the area of CO_2 measured after 40 min is (0.9 a.u.), similar to the previous case. However, the area of carbonyls band is higher than previously and the band corresponding to CH_x species shows a lower intensity. To explain this fact, the detected production of CO_2 (without CO modification) from 40 min, must be considered. This fact confirms that water participates in the gasification of adsorbed carbon, which implies a higher number of "clean" metallic sites able to adsorb CO and a lower amount of surface carbon to be hydrogenated. Therefore, we propose that water in low concentrations gasifies the C* species produced by the B way in schema 2 and consequently, the C route in this schema proceed in a lesser extent.

4. Conclusions

It has been concluded that CO interaction with the surface of a Ru/Al_2O_3 at 150 °C produces CO_2 and adsorbed carbon on the surface by the WGS and Boudouard reactions. Water in low concentrations (close to the monolayer) participates in the carbon gasification, cleaning the surface sites, and may explain the positive effect observed by some authors on the CO conversion in Fischer Trospch conditions.

However, water concentrations high enough to fill the pores of the solid restrict the CO adsorption on the metallic sites due to diffusion limitations, and explain the negative effect previously reported.

It is worth to note that the experiences analyzed in this work have been carried out in conditions very different from the real ones. At the low pressures used, the production of long chain hydrocarbons is not favored and only the hydrogenation of C* species has been observed. Working at higher pressures, an improvement of gases adsoption and chain growth are expected. In spite of used experimental conditions, interesting data regarding the behavior of the catalytic system, have been obtained. These data are of capital importance in the development of *operando* studies which permit to observed the catalyst under working conditions and can provide an approach to the complex mechanism of this reaction. The present work is the starting point to complete *operando* studies (flow, pressure and temperature, DRIFTS-MS) of the FTS currently in preparation".

Acknowledgement

The authors gratefully acknowledge the financial support from the Spanish Ministerio de Economía y Competitividad –MINECO (ENE2015-66975-C3-2R).

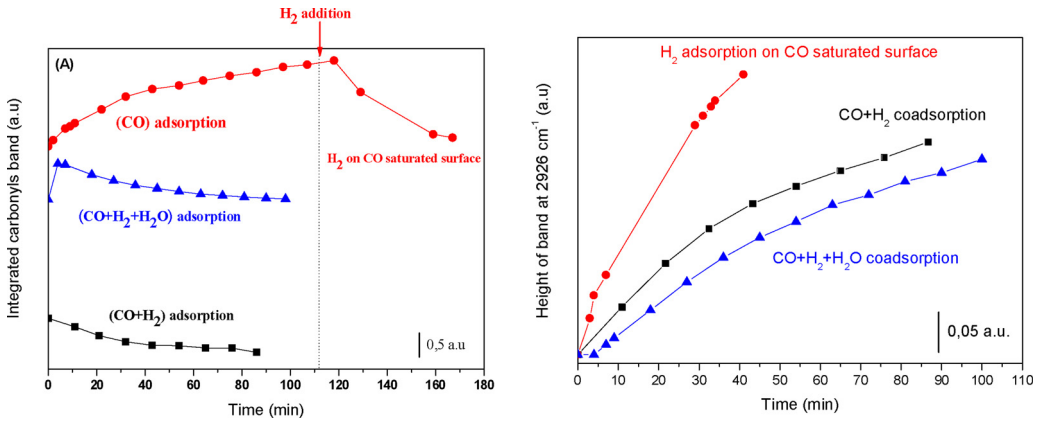

Fig. 14. Evolution of the carbonyls (~2050–2036 cm^{-1}) and ν(CH) bands with time in each one of the experiments.

References

[1] A.Y. Khodakov, W. Chu, P. Fongarland, Chem. Rev. 107 (2007) 1692–1744.
[2] M.L. Savaliya, B.D. Dhorajiya, B.Z. Dholakiya, Res. Chem. Int. (2015) 475–509.
[3] F.E.M. Farias, F.R.C. Silva, S.J.M. Cartaxo, F.A.N. Fernandes, F.G. Sales, Lat. Am. Appl. Res. 287 (4) (2007) 283–287.
[4] G. Arzamendi, P.M. Diéguez, M. Montes, J.A. Odriozola, E.F. Sousa-aguiar, L.M. Gandía, Chem. Eng. J. 160 (2010) 915–922.
[5] G.C. Visconti, E. Tronconi, G. Groppi, L. Lietti, M. Iovane, S. Rossini, R. Zennaro, Chem. Eng. J. 171 (3) (2011) 1294–1307.
[6] L.C. Almeida, F.J. Echave, O. Sanz, M.A. Centeno, J.A. Odriozola, Washcoating of metallic monoliths and microchannel reactors, Elsevier Masson SAS 175 (2010).
[7] V. Sage, N. Burke, Catal. Today 178 (2011) 137–141.
[8] O.O. James, B. Chowdhury, M. Adediran, S. Maity, RSC Adv. 2 (2012) 7347–7366.
[9] S. Shetty, A.P.J. Jansen, R.A. Van Santen, J. Am. Chem. Soc. 131 (36) (2009) 12874–12875.
[10] M. Ojeda, R. Nabar, A.U. Nilekar, A. Ishikawa, M. Mavrikakis, E. Iglesia, J. Catal. 272 (2) (2010) 287–297.
[11] R.A. van Santen, A.J. Markvoort, ChemCatChem 5 (2013) 3384–3397.
[12] F. Fischer, H. Tropsch, Brennst. Chem. 7 (1926) 97.
[13] C.F. Huo, J. Ren, Y.W. Li, J. Wang, H. Jiao, J. Catal. 249 (2) (2007) 174–184.
[14] C. Huo, Y. Li, J. Wang, H. Jiao, J. Phys. Chem. C 112 (2008) 14108–14116.
[15] B.T. Loveless, C. Buda, M. Neurock, E. Iglesia, J. Am. Chem. Soc. 135 (16) (2013) 6107–6121.
[16] R.A. Van Santen, Acc. Chem. Res. 42 (1) (2009) 57–66.
[17] G. Prieto, A. Martínez, P. Concepción, R. Moreno-Tost, J. Catal. 266 (2009) 129.
[18] J.M. González Carballo, J. Yang, A. Holmen, S. García-Rodríguez, S. Rojas, M. Ojeda, J.L.G. Fierro, J. Catal. 284 (2011) 102–108.
[19] J. P Den Breejen, P.B. Radstake, G.L. Bezemer, J.H. Bitter, V. Frøseth, A. Holmen, K.P. De Jong, J. Am. Chem. Soc. 131 (20) (2009) 7197–7203.
[20] D. Shi, J. Faria, T.N. Pham, D.E. Resasco, ACS Catal. 4 (2014) 1944–1952.
[21] C.J. Bertole, C.A. Mims, G. Kiss, J. Catal. 96 (2002) 84–96.
[22] D.D. Hibbitts, B.T. Loveless, M. Neurock, E. Iglesia, Angew. Chem. Int. Ed. 52 (47) (2013) 12273–12278.
[23] S.Y. Chin, C.T. Williams, M.D. Amiridis, J. Phys. Chem. B 110 (2006) 871–882.
[24] N. Kizhakevariam, X. Jiang, M.J. Weaver, N. Kizhakevariam, X. Jiang, M.J. Weaver, J. Chem. Phys. 9 (1994) 6750–6764.
[25] S. Krishnamoorthy, M. Tu, M.P. Ojeda, D. Pinna, E. Iglesia, J. Catal. 211 (2002) 422–433.
[27] R.A. Van Santen, I.M. Ciobica, E. Van Steen, M.M. Ghouri, Adv. Catal. 54 (2011) 127–187.
[28] E. Iglesia, Appl. Catal. A Gen 161 (1–2) (1997) 59–78.
[29] E. van Steen, M. Claeys, M.E. Dry, J. van de Loosdrecht, E.L. Viljoen, L. Visagie, J. Phys. Chem. B 109 (2005) 3575–3577.
[30] S. Storsæter, Ø. Borg, E.A. Blekkan, A. Holmen, J. Catal. 231 (2005) 405–419.
[31] G.W. Huber, C.G. Guymon, T.L. Conrad, B.C. Stephenson, C.H. Bartholomew, Hydrothermal stability of Co/SiO2 Fischer-Tropsch synthesis catalysts, Elsevier Masson SAS 139 (2001).
[32] Y. Zhang, D. Wei, S. Hammache, J.G. Goodwin, J. Catal. 188 (1999) 281–290.
[33] W. Ma, G. Jacobs, D.E. Sparks, R.L. Spicer, B.H. Davis, J.L.S. Klettlinger, C.H. Yen, Catal. Today 228 (2014) 158–166.
[34] M. Lualdi, S. Lögdberg, M. Boutonnet, S. Järås, Catal. Today 214 (2013) 25–29.
[35] M. Claeys, E. van Steen, Catal. Today 71 (3–4) (2002) 419–427.
[36] A.K. Dalai, B.H. Davis, Appl. Catal. A Gen. 348 (1) (2008) 1–15.
[37] A.K. Dalai, T.K. Das, K.V. Chaudhari, G. Jacobs, B.H. Davis, Appl. Catal. A Gen. 289 (2) (2005) 35–142.
[38] C.J. Bertole, G. Kiss, C.A. Mims, J. Catal. 223 (2004) 309–318.
[39] L. Liu, Sun G, C. Wang, J. Yang, C. Xiao, H. Wang, D. Ma, Y. Kou, Catal. Today 183 (2012) 136–142.
[40] J.M. González Carballo, E. Finocchio, S. García, S. Rojas, M. Ojeda, G. Busca, J.L.G. Fierro, Catal. Sci. Technol. 1 (6) (2011) 1013–1023.
[41] P.A. Gerakines, W.A. Schutte, J.M. Greenberg, E.F. Dishoeck, Astron. Astrophys. 296 (1995) 810–818.
[42] K. Hadjiivanov, J.C. Lavalley, J. Lamotte, F. Maugé, J. Saint-Just, M. Che, J. Catal. 176 (2) (1998) 415–425.
[43] O. Dulaurent, M. Nawdali, A. Bourane, Appl. Catal. A 201 (2000) 271–279.
[44] K. Okabe, K. Murata, M. Nurunnabi, Y. Liu, J. Jpn. Pet. Inst. 52 (3) (2009) 139–142.
[45] J.A. Delgado, C. Claver, S. Castillon, D. Curulla-Ferre, C. Godard, ACS Catal. 5 (8) (2015) 4568–4578.
[46] H. Wise, J.G. Mccarty, Surf. Sci. 133 (1983) 311–320.
[47] G.H. Yokomizo, C. Louis, A.T. Bell, J. Catal. 120 (1989) 15–21.
[48] A. Michaelides, A. Alavi, D.A. King, J. Am. Chem. Soc. 125 (2003) 2746–2755.
[49] P.J. Feibelman, Partial dissociation of Water on Ru (0001), Science 295 (2002) 99–102.
[50] G. Held, D. Menzel, Surf. Sci. 316 (1994) 92–102.
[51] M. Nakamura, M. Ito, Chem. Phys. Lett. 325 (2000) 293–298.
[52] S.D. Senanayake, D. Stacchiola, P. Liu, C.B. Mullins, J. Hrbek, J. Phys. Chem. C 113 (2) (2009) 19536–19544.
[53] P. Panagiotopoulou, D.I. Kondarides, X.E. Verykios, J. Phys. Chem. C 115 (4) (2001) 1220–1230.
[54] S.Z. Todorova, G.B. Kadinov, Res. Chem. Intermed. 28 (4) (2002) 291–301.
[55] P. Bazin, O. Saur, J.C. Lavalley, M. Daturi, G. Blanchard, Phys. Chem. Chem. Phys. 7 (2005) 187–194.
[56] Y. Kobori, S. Naito, T. Onishi, K. Tamaru, J. Chem. Soc. Chem. Comm. 3 (1981) 92–93.
[57] A. Vimont, J.C. Lavalley, A. Sahibed-Dine, C.O. Arean, M.R. Delgado, M. Daturi, J. Phys. Chem. B 109 (2005) 9656–9664.
[58] C. Morterra, A. Zecchina, S. Coluccia, A. Chiorino, J. Chem. Soc., Faraday Trans. I. 7 (73) (1977) 1544–1560.
[59] K. Föttinger, R. Schlögl, G. Rupprechter, Chem. Commun. 3 (2008) 320–322.
[60] Z. Mei, Y. Li, M. Fan, M.D. Argyle, J. Tang, Int. J. Hydrogen Energy 39 (27) (2014) 14808–14816.
[61] W. Xu, R. Si, S.D. Senanayake, J. Llorca, H. Idriss, D. Stacchiola, J.C. Hanson, J.A. Rodriguez, J. Catal. 291 (2012) 117–126.
[62] C. Morterra, G. Magnacca, Catal. Today 27 (3–4) (1996) 497–532.
[63] T. Onfroy, W.C. Li, F. Schüth, H. Knözinger, Phys. Chem. Chem. Phys. 11 (19) (2009) 3671–3679.
[64] E. Guglielminotti, E. Giamello, F. Pinna, G. Strukul, S. Martinengo, L. Zanderighi, J. Catal. 149 (1994) 422–436.
[65] I. Glassman, R.A. Yetter, Combustion (2008) 1–773.
[66] M.I. Lester, B.V. Pond, M.D. Marshall, D.T. Anderson, L.B. Harding, A.F. Wagner, Faraday Discuss. 118 (2001) 373–385.
[67] J.A. Rodriguez, S.D. Senanayake, D. Stacchiola, P. Liu, J. Hrbek, Acc. Chem. Res. 47 (3) (2014) 773–782.
[68] A. Politano, G. Chiarello, RSC Adv. 4 (2014) 45641–45646.
[69] R.A. Dalla-betta, M. Shelef, J. Catal. 48 (1977) 111–119.
[70] I.M. Ciobica, A.W. Kleyn, R.A. Van Santen, J. Phys. Chem. B 107 (1) (2003) 164–172.
[71] C.E. Nanayakkara, J.K. Dillon, V.H. Grassian, J. Phys. Chem. C 118 (2014) 25487–25495.
[72] J.M.G. Carballo, E. Finocchio, S. García-Rodriguez, M. Ojeda, J.L.G. Fierro, G. Busca, S. Rojas, Catal. Today 214 (2013) 2–11.
[73] D.L. King, J. Catal. 51 (3) (1978) 386–397.
[74] I.A.W. Filot, R.A. Van Santen, E.J.M. Hensen, Angew. Chem. Int. Ed. 53 (47) (2014) 12746–12750.
[75] J. Szanyi, J.H. Kwak, Phys. Chem. Chem. Phys. 16 (29) (2014) 15117–15125.